GSA Data Repository 2015335

I. Scanning electron microscopy methods.

External BSE imaging of all three grains was done using scanning electron microscopy (SEM) with a Hitachi S3400 W-filament SEM at the University of Wisconsin-Madison.

For grains 13DG08-24 and 14VD80-205, further SEM analysis was conducted using a Tescan MIRA3 field emission gun (FEG) SEM at the Microscopy and Microanalysis Facility at Curtin University. The FEG-SEM was used for panchromatic cathodoluminescence (CL) imaging, and electron backscatter diffraction (EBSD). Automated EBSD maps of regions of interest were generated by indexing of electron backscatter diffraction patterns on user-defined grids, and were collected for zircons 24 and 205. Whole-grain maps at 0.25 µm (grain 24) and 1.0 µm (grain 205) step size were made. EBSD analyses were collected with a 20 kV accelerating voltage, 70° sample tilt, 20.5 mm working distance, and 18 nA beam intensity. Electron backscatter patterns were collected with a Nordlys Nano high resolution detector and Oxford Instruments Aztec system using routine data acquisition and noise reduction settings (Table DR1; Reddy et al., 2007).

For grain 07VD07-3, further SEM analysis was conducted using a Hitachi SU6600 FEG-SEM in the Zircon and Accessory Phase Laboratory at Western University. Cathodoluminescence (CL) images were collected with a Gatan Chroma CL detector operating at 10 kV. EBSD maps were collected with an Oxford Instruments Nordlys EBSD detector using the methodology of Moser et al. (2011). A full grain EBSD map using ~500 nm step size was made of grain 07VD07-3.

EBSD maps and pole figures for all three grains were processed using the Tango and Mambo modules in the Oxford Instruments/HKL Channel 5 software package.

EBSD analysis conditions are shown in Table DR1.

II. SHRIMP ion microprobe methods.

Zircons 13DG08-24 and 14VD80-05 were analyzed in Au-coated epoxy mounts in March, 2015 using the SHRIMP II at the John de Laeter Center, Curtin University. The analytical procedures for the Curtin consortium SHRIMP II have been described by De Laeter and Kennedy (1998), and Kennedy and De Laeter (1994) and are similar to those described by Nelson (1997) and Williams (1998). A 20 μm diameter spot was used, with a mass-filtered O_2^--primary beam of 1.7-2.1 nA on those zircons. A complete analysis consisted of six cycles of measurements at each mass [$^{196}(Zr_2O)$, ^{204}Pb, $^{204.045}Pb(bkg)$, ^{206}Pb, ^{207}Pb, ^{208}Pb, ^{238}U, $^{248}(ThO)$, and $^{254}(UO)$]. Zircon U/Pb concentration standards used were M257 [U] = 840 ppm (Nasdala et al, 2008), and R33, $^{238}U/^{206}Pb$ age = 419 Ma (Black et al., 2004). The $^{207}Pb/^{206}Pb$ standard used to monitor instrument induced mass fractionation was OGC zircon (3467+/-3 Ma; Stern et al. 2009). The $^{207}Pb/^{206}Pb$ dates obtained on OGC zircons during the SHRIMP session matched the $^{207}Pb/^{206}Pb$ standard age within uncertainty and no fractionated correction was warranted. Standard results for the two analytical runs were (Pb/U calibration error in 1σ%): 0.31% for 13DG08-24, and 0.26% for 14VD80-205.

Zircon 07VD06-3 was analyzed in an Au-coated epoxy mount in October 2010, using the SHRIMP-RG (reverse geometry) ion microprobe co-operated by U.S. Geological Survey and Stanford University in the SUMAC facility at Stanford University. Zircon 07VD07-3 was cast in epoxy, ground and polished to a 1-micron finish on a 25 mm diameter by 4 mm thick disc. The mount was washed with a 1N HCl solution and thoroughly rinsed in distilled water, dried in a vacuum oven, and coated with Au. Mounts are typically outgassed in a loading chamber at low pressure (10^{-7} torr) for several hours before being moved into the source chamber of the SHRIMP-RG. Secondary ions were generated from the target spot with an O_2^- primary ion beam varying from 4-6 nA. The primary ion beam produces a spot with diameter of 20 microns and a depth of 1-2 microns for an analysis time of 9-12 minutes. The full set of analyzed peaks begins with a high mass normalizing species ($^{90}Zr_2{}^{16}O^+$), followed by $^{204}Pb^+$, a background measured at 0.050 mass units above $^{204}Pb^+$, $^{206}Pb^+$, $^{207}Pb^+$, $^{208}Pb^+$, $^{238}U^+$, $^{232}Th^{16}O^+$ and $^{238}U^{16}O^+$ and $^{232}Th^+$, and $^{270}UO_2$. A complete analysis consisted of five cycles of measurements at each mass Measurements are made at mass resolutions of M/ΔM = 7500-8500 (10% peak height), which eliminates all interfering molecular species. The instrumental design provides very clean backgrounds and combined with the high mass resolution, the HCl washing of the mount, and rastering the primary beam for 90-180 seconds over the area to be analyzed before data are collected, assures that any counts found at mass of $^{204}Pb^+$ are actually from Pb in the zircon and not surface contamination. Concentration data for U and Th were standardized against zircon standard MAD-green (4196 ppm U) (Mazdab and Wooden, 2006). Age data were standardized against zircon R33, whose age is 419 Ma (Black et al., 2004), which were analyzed repeatedly throughout the analytical session. The external spot-to-spot uncertainty for R33 was 1.93%.

Data reduction for geochronology followed the methods described by Williams (1998) and Ireland and Williams (2003), and used the MS Excel add-in Squid 1, Squid 2, and Isoplot programs of Ludwig (2001a,2001b, 2003, 2009).

SHRIMP Results are shown in Table DR2.

III. Additional images of zircon 13DG08-24.

A: BSE image showing planar fractures visible on the exterior surface.
B: Cathodoluminescence image of the polished surface, showing fractures and complicated zonation. Scale bar = 50 µm.

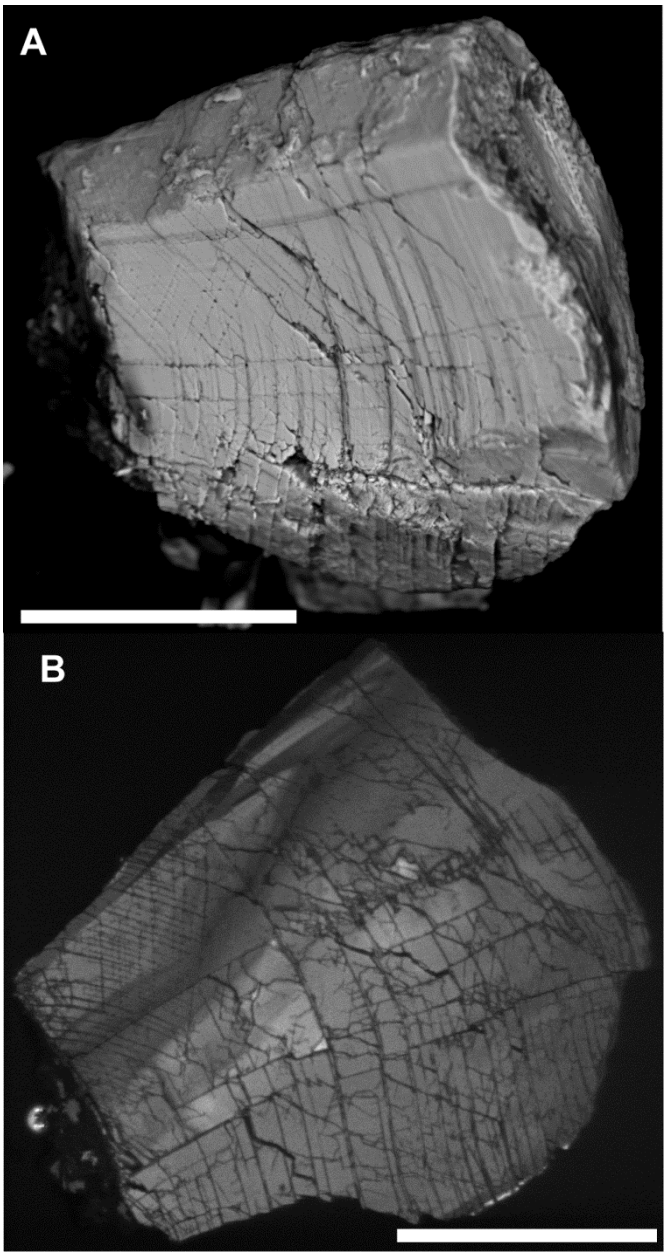

IV. Additional EBSD information for zircon 13DG08-24.

A: Map showing crystallographic orientation for zircon 24 (with an inverse pole figure color scheme). Four sets of microtwins (t) are labeled (t1-t4).
B: Pole figures of all data from zircon 24. C: Pole figures for the host zircon. D: Pole figures for the microtwins, labeled t1-t4 (labels omitted in {112} for clarity). Stereonets are equal area, lower hemisphere projections.

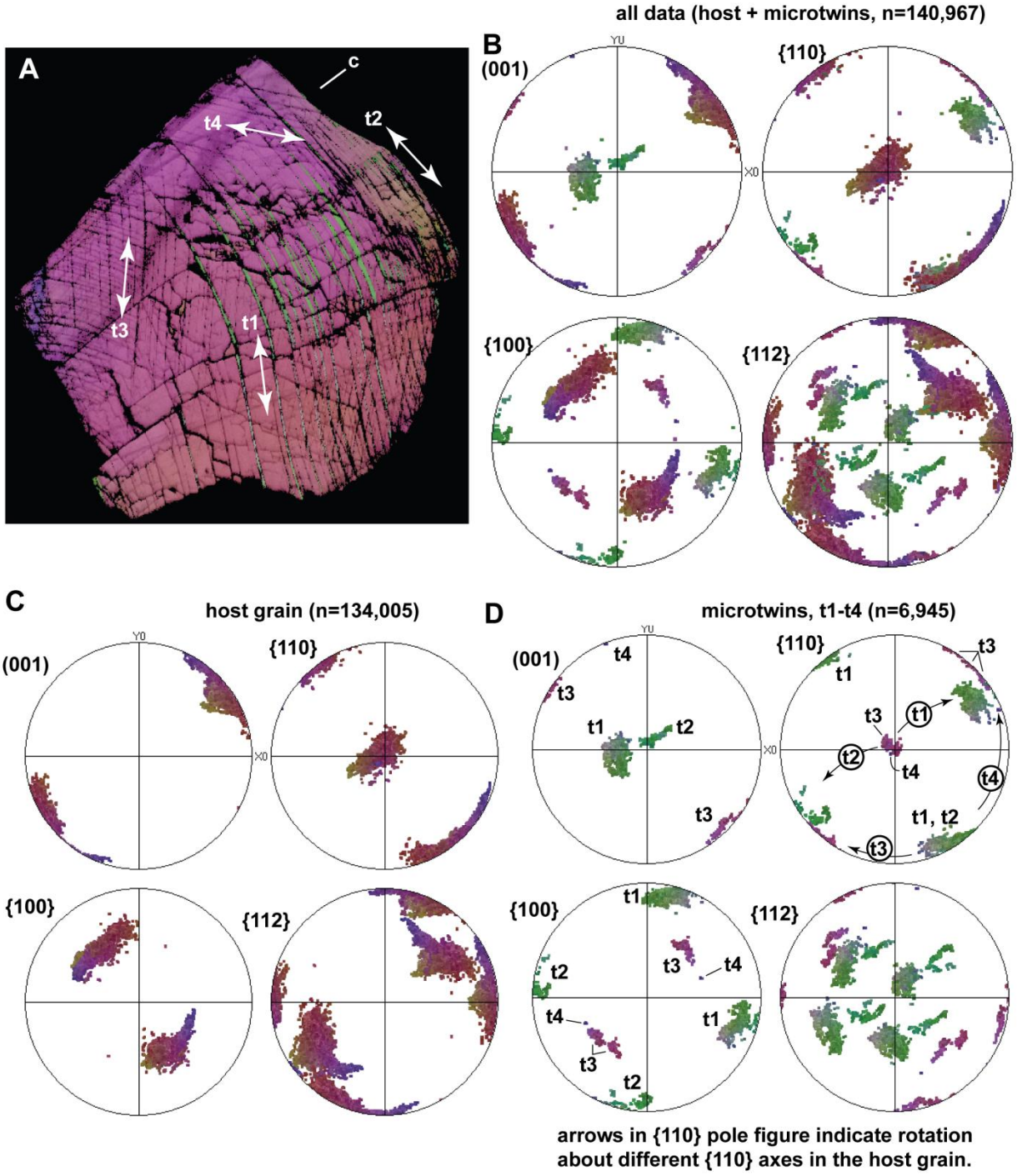

V. Misorientation axis plots for zircons 24, 3, and 205.

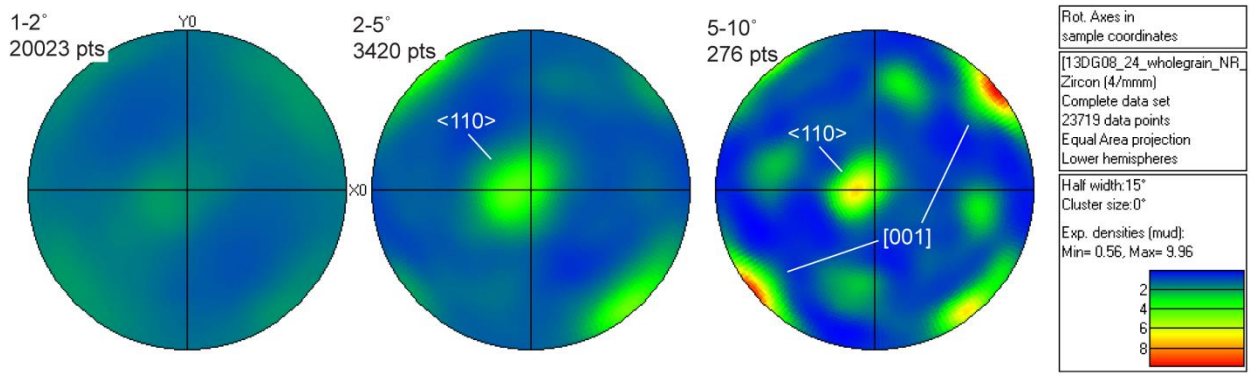

Zircon 13DG08-24 (above): Stereonets showing misorientation axes for low angle grain boundaries (whole grain). The dominant misorientation axes are <110> and [001].

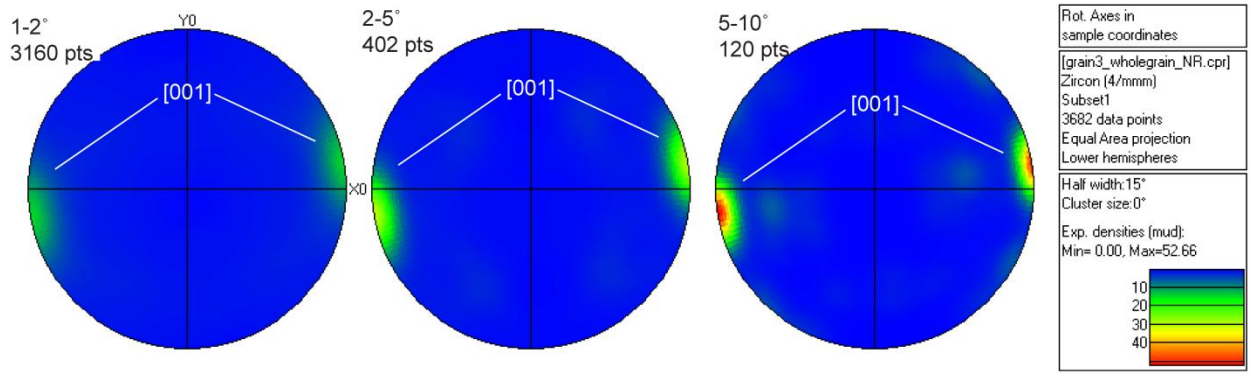

Zircon 07VD07-3 (above): Stereonets showing misorientation axes for low angle boundaries in the igneous domain (neoblasts excluded). The dominant misorientation axis in all three groups is [001] (labeled).

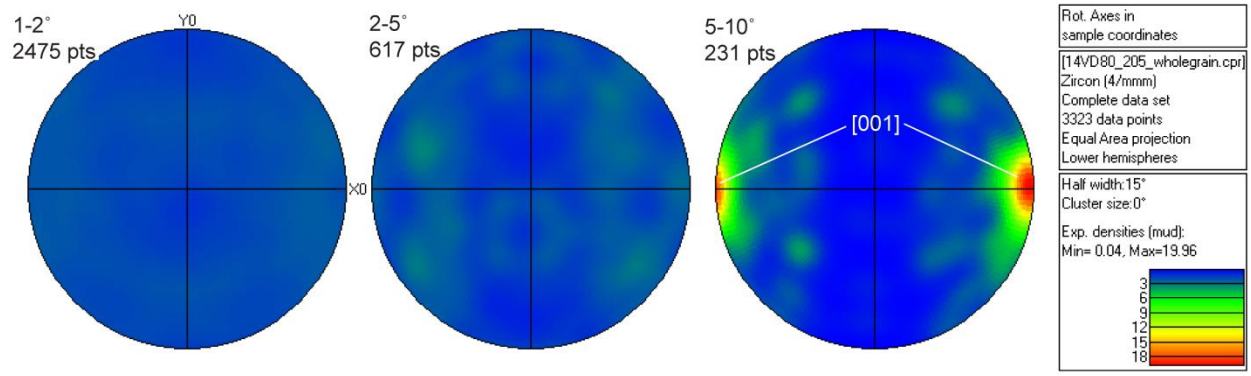

Zircon 14VD80-205 (above): Stereonets showing misorientation axes for low angle boundaries (whole grain). No dominant misorientation axis is present in the 1-2° and 2-5° groups; for low angle boundaries from 5-10°, [001] is the dominant axis (labeled). Other misorientation axes detected include <211>, <112>, <201>, <210>, and <111>.

VI. Internal misorientation of neoblasts in zircon 07VD07-3.

The map below was constructed from EBSD data, and is color coded to illustrate mean internal misorientation within individual neoblasts as well as the host zircon. The host zircon is treated as a single domain (excluding the microtwins), and shows maximum internal misorientation of 8° (red). The mean internal misorientation for individual neoblasts is <2° (blue to bluish green). One neoblast (down and to the right of center, slightly more yellow) preserves a mean internal misorientation of ~4°. The histogram below the EBSD map shows the correlation of mean internal misorientation to color.

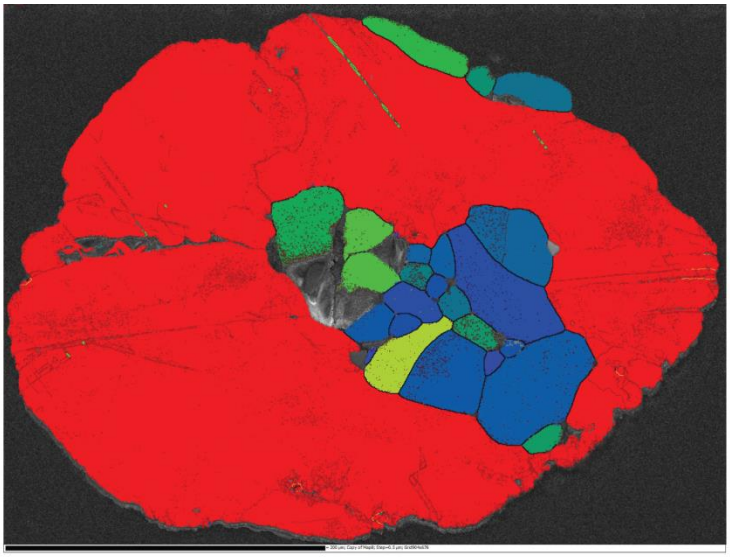

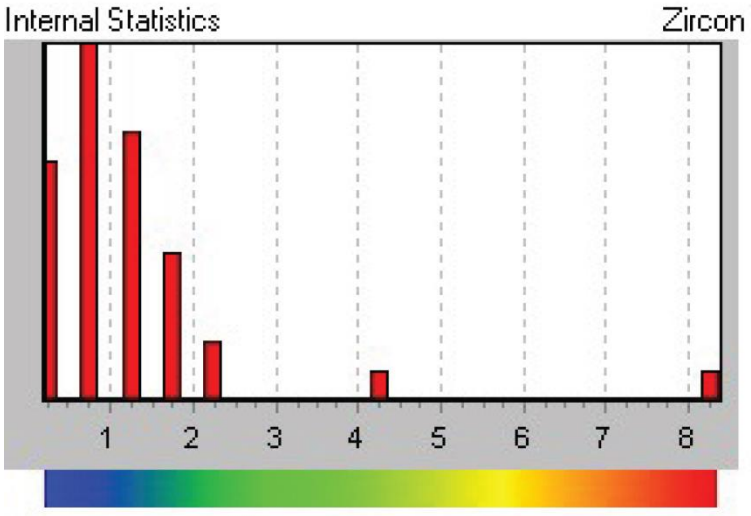

VII. Additional sample location information.

Sample 14VD80 was collected from beach sand on the Atlantic coast of South Africa at the mouth of the Orange River (Montalvo, 2015). GPS coordinates: S28° 38.254', E16° 27.696.

Sample 13DG08 was separated from a sample of glacial tillite exposed in the collar of the Vredefort Dome (Pincus, 2015). GPS coordinates: S26° 52.729', E27° 14.947.

Sample 07VD07 was collected in modern alluvium from the Rietspruit, a small stream draining the core of the Vredefort Dome impact structure. GPS coordinates for this grain are given in Cavosie et al. (2010).

VIII. Data Repository References

Black L. P., Kamo S. L., Allen C. M., Davis D. W., Aleinikoff J. N., Valley J. W., Mundil R., Campbell I. H., Korsch R. J., Williams I. S. and Foudoulis C., 2004, Improved $^{206}Pb/^{238}U$ microprobe geochronology by the monitoring of a trace element- related matrix effect: SHRIMP, ID-TIMS, LA-ICPMS and oxygen isotope documentation for a series of zircon standards: Chemical Geology, v. 205, p. 115–140.

Cavosie A. J., Quintero R. R., Radovan H. A. and Moser D., 2010, A record of ancient cataclysm in modern sand: shock microstructures in detrital minerals from the Vaal River, Vredefort Dome, South Africa: GSA Bulletin, v. 112, p. 1968–1980.

De Laeter J.R. and Kennedy A.K., 1998, A double focussing mass spectrometer for geochronology: International Journal of Mass Spectrometry, v. 178, pp. 43–50.

Ireland, T.R., Williams, I.S., 2003, Considerations in zircon geochronology by SIMS: Reviews in Mineralogy and Geochemistry, v. 53, p. 215-241.

Kennedy, A.K., de Laeter, J.R., 1994, The performance characteristics of the WA SHRIMP II ion microprobe. In: Eighth International Conference on Geochronology, Cosmochronology and Isotope Geology. Berkeley, USA. Abstracts Vol., U.S. Geological Survey Circular, 1107, 166.

Ludwig K. R., 2001a, Squid 1.02: A User's Manual: Berkeley Geochronology Center Special Publication No. 1a.

Ludwig K. R., 2001b, User's Manual for Isoplot 3.00: A Geochronological Toolkit for Microsoft Excel: Berkeley Geochronology Center Special Publication No. 4.

Ludwig, K.R., 2003, Isoplot 3.0. A Geochronological Toolkit for Microsoft Excel: Berkeley Geochronology Center Special Publication No. v. 4, 70 pp.

Ludwig, K.R., 2009, SQUID II., a user's manual: Berkeley Geochronology Center Special Publication 2, 2455 Ridge Road, Berkeley, CA 94709, USA 22.

Mazdab, F. K., and Wooden, J. L., 2006, Trace element analysis in zircon by ion microprobe (SHRIMP–RG): technique and applications: Geochimica et Cosmochimica Acta, v. 70(18), Supp. 1, A405.

Montalvo, S. D., 2015, Detrital shocked zircons in the Orange River, South Africa. Master's Thesis, University of Puerto Rico-Mayagüez, 133p.

Moser D. E., Cupelli C. L., Barker I. R., Flowers R. M., Bowman J. R., Wooden J. and Hart J. R., 2011, New zircon shock phenomena and their use for dating and reconstruction of large impact structures revealed by electron nanobeam (EBSD, CL, EDS) and isotopic U–Pb and (U–Th)/He analysis of the Vredefort Dome: Canadian Journal of Earth Science, v. 48, p. 117–139.

Nasdala, L., Hofmeister, W., Norberg, N., Mattinson, J.M., Corfu, F., Dörr, W., Kamo, S.L., Kennedy, A.K., Kronz, A., Reiners, P.W., Frei, D., Kosler, J., Wan, Y., Götze, J., Häger, T., Kröner, A., and Valley, J.W., 2008, Zircon M257- a homogeneous natural reference material for the ion microprobe U-Pb analysis of zircon: Geostandards and Geoanalytical Research: v.32, p. 247–265.

Nelson, D.R., 1997, Compilation of SHRIMP U–Pb zircon geochronology data, 1996. Geological Survey of Western Australia Record No. 1997/2.

Pincus, M.R, 2015, Detrital shocked minerals in the Paleozoic Dwyka Group, South Africa. Master's Thesis, University of Puerto Rico-Mayagüez, 100p.

Reddy S. M., Timms N. E., Pantleon W., and Trimby T., 2007, Quantitative characterization of plastic deformation of zircon and geological implications: Contributions to Mineralogy and Petrology, v. 153, p. 625–645.

Stern, R.S., Bodorkos S., Kamo S. L., Hickman, A. H., and Corfu F. (2009). Measurement of SIMS instrumental mass fractionation of Pb-isotopes during zircon dating: Geostandards and Geoanalytical Research, v. 33, p. 145-168.

Williams I. S., 1998, U–Th–Pb geochronology by ion microprobe. In Applications of Microanalytical Techniques to Understanding Mineralizing Processes, vol. 7 (eds. M. A. Mckibben, W. C. Shank and W. I. Ridley). Reviews in Economic Geology, pp. 1–35.

Table DR1. EBSD analysis conditions.

SEM Model (Curtin University)	Tescan Mira3 FEG-SEM	
Grain	Zircon 24	Zircon 205
Shown in figure	2A, DR	3G,4C,4D, DR
Acquisition speed (Hz)	40	40
Background (frames)	64	64
Binning	4 x 4	4 x 4
Gain	High	High
Hough resolution	60	60
Band detection min/max	18/165	22/148
Average mean angular deviation (zircon)	0.45	0.35
X steps	554	563
Y steps	378	236
Step distance (nm)	250	1000
Noise reduction – 'wildspike'	Yes	Yes
n neighbour zero solution extrapolation	0	0
Kuwahara Filter	No	No
Tescan Mira3 FEG-SEM settings		
EBSD system	Nordlys Detector - Aztec	
Carbon coat (<5nm)	Yes	Yes
Acc. voltage (kV)	20	20
Working distance (mm)	20.5	20.5
Tilt (degrees)	70	70

SEM Model (Western University)	Hitachi SU6600
Grain	Zircon 3
Shown in figure	3C,4A,4B, DR
Acquisition speed (Hz)	19
Background (frames)	65
Binning	4x4
Gain	High
Hough resolution	60
Band detection min/max	5/7
Average mean angular deviation (zircon)	0.38
X steps	904
Y steps	676
Step distance (nm)	500
Noise reduction – 'wildspike'	No
n neighbour zero solution extrapolation	No
Kuwahara Filter	No
Hitachi SU FEG-SEM settings	
EBSD system	Nordlys Detector
Carbon coat (<5nm)	Yes
Acc. voltage (kV)	20
Working distance (mm)	19
Tilt (degrees)	70

Table DR2. Zircon U-Th-Pb isotopic data.

	micro-structure	CL zoning[1]	U (ppm)	Th (ppm)	Th/U	% comm[1] ^{206}Pb	$^{204}Pb/^{206}Pb$	$^{208}Pb^*/^{232}Th$	$^{207}Pb^*/^{235}U$	$^{206}Pb^*/^{238}U$	$^{207}Pb^*/^{206}Pb^*$	$^{206}Pb^*/^{238}U$ Age (Ma)[2]	$^{207}Pb^*/^{206}Pb^*$ Age (Ma)[2]	% disc[1]
spot	Grain 07VD07-3													
1	PM[1], t[1]	oscillatory	125	133	1.10	0.11	0.00009	0.1419±0.0035	15.07±0.41	0.5259±0.0095	0.20787±0.00427	2724±40	2889±34	6
3	PM, t	oscillatory	82	67	0.84	0.06	0.00004	0.1407±0.0064	13.92±0.41	0.5111±0.0102	0.19754±0.00398	2661±48	2806±32	5
6	PM, t	oscillatory	126	133	1.09	0.05	0.00004	0.1409±0.0032	15.28±0.32	0.5215±0.0094	0.21259±0.00252	2705±38	2925±20	8
2	neoblast	bright	44	42	0.99	0.24	0.00016	0.1024±0.0048	6.13±0.27	0.3626±0.0109	0.12255±0.00398	1995±52	1994±58	0
4	neoblast	bright	46	43	0.97	0.62	0.00041	0.0970±0.0069	5.77±0.30	0.3500±0.0105	0.11957±0.00493	1935±50	1950±74	1
5	neoblast	bright	37	24	0.67	0.57	0.00037	0.0980±0.0072	6.02±0.33	0.3612±0.0116	0.12084±0.00526	1988±56	1968±78	-1
spot	Grain 13DG08-24													
1	PM, t	disturbed	368	277	0.75	4.81	0.00266	0.0295±0.0025	2.62±0.15	0.1050±0.0051	0.18123±0.00542	644±30	2664±50	79
2	PM, t	disturbed	515	317	0.62	3.70	0.00204	0.0422±0.0065	3.14±0.42	0.1086±0.0137	0.20967±0.00906	665±80	2903±70	81
3	PM, t	disturbed	472	222	0.47	6.61	0.00366	0.0165±0.0030	1.42±0.09	0.0581±0.0015	0.17773±0.01112	364±10	2632±104	88
4	PM, t	disturbed	1063	502	0.47	9.02	0.00499	0.0095±0.0021	0.81±0.10	0.0312±0.0033	0.18733±0.01348	198±20	2719±118	94
spot	Grain 14VD80-205.													
1	core	oscillatory	165	109	0.66	0.07	0.00004	0.0943±0.0034	5.17±0.16	0.3387±0.0092	0.11077±0.00178	1880±44	1812±28	-4
2	rim	dark	774	15	0.02	-0.04	-0.00003	0.0610±0.0083	1.74±0.05	0.1727±0.0044	0.07339±0.00084	1027±24	1025±24	0

[1] PM = planar microstructure; t = microtwin; CL = cathodoluminescence; comm = common; disc = discordance.

[2] Age in Ma. Uncertainty in ages and isotope ratios is listed at 2σ.

* indicates a ^{204}Pb corrected Pb value.